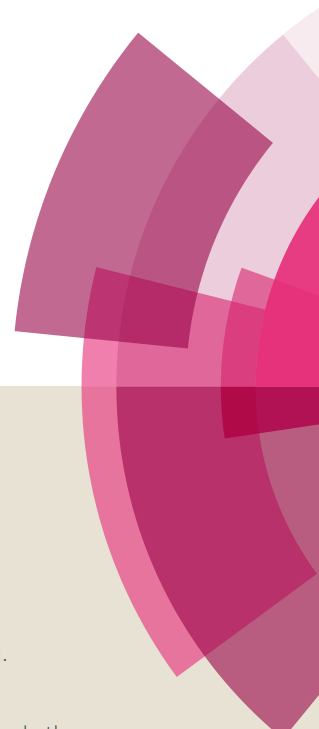


NJC

Accepted Manuscript



This article can be cited before page numbers have been issued, to do this please use: J. Custodio, L. Michelini, M. Castro, W. Fonseca Vaz, B. J. Neves, P. Cravo, F. Barreto, M. O. de Moraes, C. Perez and H. Napolitano, *New J. Chem.*, 2018, DOI: 10.1039/C7NJ03523C.



This is an Accepted Manuscript, which has been through the Royal Society of Chemistry peer review process and has been accepted for publication.

Accepted Manuscripts are published online shortly after acceptance, before technical editing, formatting and proof reading. Using this free service, authors can make their results available to the community, in citable form, before we publish the edited article. We will replace this Accepted Manuscript with the edited and formatted Advance Article as soon as it is available.

You can find more information about Accepted Manuscripts in the [author guidelines](#).

Please note that technical editing may introduce minor changes to the text and/or graphics, which may alter content. The journal's standard [Terms & Conditions](#) and the ethical guidelines, outlined in our [author and reviewer resource centre](#), still apply. In no event shall the Royal Society of Chemistry be held responsible for any errors or omissions in this Accepted Manuscript or any consequences arising from the use of any information it contains.

ARTICLE

Structural Insights on a Novel Anticancer Sulfonamide Chalcone

Jean M. F. Custodio^{a,b}, Lidiane J. Michelini^a, Mirian Rita C. de Castro^a, Wesley F. Vaz^b, Bruno J. Neves^c, Pedro V. L. Cravo^{c,d}, Francisco S. Barreto^e, Manoel O. M. Filho^e, Caridad N. Perez^a and Hamilton B. Napolitano^{b,c}

Received 00th January 20xx,
Accepted 00th January 20xx

DOI: 10.1039/x0xx00000x

www.rsc.org/

Natural products have stood out due to their wide range of biological activities. Among the various naturally occurring classes, we can highlight chalcones, sulfonamides and hybrid compounds formed by both. Although many pharmacological activities of these classes of compounds are known, new ones have arisen lately and require detailed structural and biological analyses. Herein, we report the synthesis and structural elucidation of a novel sulfonamide chalcone 2,5-dichloro-*N*-{3-[(2E)-3-(4-nitrophenyl)prop-2-enoyl]phenyl}benzenesulfonamide (BSC) by Single Crystal X-ray Diffraction and spectroscopy analysis (Infrared, NMR and Mass Spectroscopy). Topology was determined through Hirshfeld surfaces analysis and electrostatic potential map, while the energy of frontier molecular orbitals evaluated the stability of BSC. Additionally, the cytotoxicity of the title compound was evaluated through the MTT colorimetric method. We show that the BSC compound has a planar conformation in its chalcone portion, which is further corroborated by the low angle between the aromatic rings (5.23°). In addition, intermolecular interactions of type C-H...O and N-H...O make up a dimeric supramolecular arrangement. An inverse virtual screening approach allowed identifying potential biological applications for BSC, which indicated that BSC might interact with binding sites of the RAR α and RAR β . Consequently, BSC was experimentally evaluated against three cancer cell lines, and was shown to hold potent anticancer activity. In addition, a cytotoxic effect was observed for all strains, which was more pronounced for HCT-116, a colon cancer cell line.

Introduction

Natural products (NPs) have traditionally formed the backbone of modern drug discovery programs¹. Recently it was shown that 28% of all approved drugs are either NPs (15%) or NP-inspired compounds (13%)². In other words, the exploration of NPs offers a remarkable opportunity to identify interesting chemical scaffolds for drug discovery by providing chemically diverse compounds. To expand on their success, and explore areas of chemical space not covered by biosynthesis, there has been a movement to develop synthetic compounds that have complexity comparable to that of NPs. This strategy can provide prototypes that represent the best of both chemical spaces: structurally diverse molecules with physicochemical properties analogous to those of NPs, accessed as rapidly as the other synthetic compounds³.

Among the most promising NPs, chalcones (1,3-diphenyl-2-propen-1-ones) have gained attention due to the large number

of replaceable hydrogens that allow generating a large number of derivatives, ease of synthesis, and a variety of promising biological activities⁴. These privileged structures have been widely studied as anti-inflammatory⁵, anti-oxidant⁶, anti-obesity⁷, anti-protozoal⁸, hypnotic⁹, anti-histaminic¹⁰, anti-spasmodic¹¹, anticancer¹², anti-gout¹³, etc.

Moreover, sulfonamide (-SO₂NHR-, or their closely related variants, such as thiosulfonyl, sulfonate, sulfamate) constitutes an important moiety of synthetic drugs, with several types of pharmacological agents possessing antibacterial¹⁴, antimalarial¹⁵, diuretic¹⁶, hypoglycemic¹⁷, anticonvulsant^{18,19}, antirheumatic^{20,21}, and antiretroviral²² activity, among others. More specifically, chalcones that have chlorine and nitro linkers exhibit appreciable antitumor activities as suppressors of the p53 protein²³⁻²⁵. Therefore, for this work chlorine and nitro substituents were chosen from the aromatic rings. It is interesting to note that the chemical space of approved drugs is composed of a small number of privileged building blocks, recurrently found in potent drug molecules, and the sulfonamide moiety is one of them.

Based on this perspective, molecules that contain sulfonamide and chalcone moieties could lead to the new hybrid architectures with improved biological profiles. Under this premise, the aim of this study was the synthesis and structural elucidation in terms of lengths and bond angles, intra and intermolecular interactions and supramolecular arrangements of the hybrid molecule 2,5-dichloro-*N*-{3-[(2E)-3-(4-nitrophenyl)prop-2-enoyl]phenyl}benzenesulfonamide (BSC)

^aInstituto de Química, Universidade Federal de Goiás, Goiânia, GO, Brazil

^bCiências Exatas e Tecnológicas, Universidade Estadual de Goiás, Anápolis, GO, Brazil

^cPrograma de Pós-Graduação em Sociedade, Tecnologia e Meio Ambiente, Centro Universitário de Anápolis, Anápolis, GO, Brazil

^dInstituto de Higiene e Medicina Tropical, Universidade Nova de Lisboa, Lisboa, Portugal

^eFaculdade de Medicina, Universidade Federal do Ceará, Fortaleza, CE, Brazil

Electronic Supplementary Information (ESI) available: [details of any supplementary information available should be included here]. See DOI: 10.1039/x0xx00000x

Further, their biological activities were assessed by integration of an *in silico* target fishing approach and biological assays.

Experimental and computational procedures

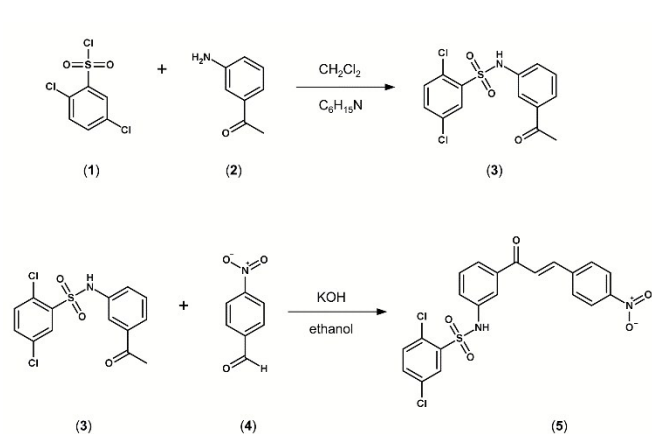
Materials and Method

Synthesis. Acetophenone sulfonamide (**3**) was synthesized using a 50 mL round bottom flask. 2,5-dichlorobenzenesulfonyl chloride (**1**, 1.0 mmol) was simultaneously added to 3-aminoacetophenone (**2**, 1.0 mmol) using triethylamine (C₆H₁₅N) as catalyst and dichloromethane (CH₂Cl₂, 15 mL). The reaction was kept under stirring and reflux for 4 hours. Subsequently, the precipitate could dry and recrystallized in ethanol. **Yield:** 50%.

Boiling point: 165-167 °C. **¹H RMN (DMSO-d₆, 500 MHz):** (500MHz – DMSO-D6): (N-H) δ = 2.67 (s, 1H), (COCH₃) = 2.49 (s, 3H), H₃' = 6.54 (ddd, 1H, J = 7, 0, 1.2 Hz), H₄' = 7.20 (ddd, 1H, J = 1.10, 0.60, 7.0 Hz), H₅' = 6.75 (ddd, 1H, J = 0.50, 1.2, 7.0 Hz), H₆' = 7.56 (ddd, 1H, J = 1.20, 7.0, 1.5 Hz), H₉' = 7.40 (ddd, 1H, J = 0.40, 1.10, 7.25 Hz), H₁₀' = 7.24 (dd, 1H, J = 1.5, 6.9, Hz), H₁₂' = 8.0 (dd, 1H, J = 1.5, 6.9 Hz). **IV (cm⁻¹):** 3081 (N-H), 1649 (C=O), 1578 (N-H), 1496 (C=O), 1360 (S=O), 1249 (C-N), 1179 (S=O) e 821 (C-Cl). **EM (m/z):** 341.97685.

Equimolar amounts of **3** (1.0 mmol) and p-nitrobenzaldehyde (**4**, 2.0 mmol) were dissolved in ethanol (10 mL) and concentrated potassium hydroxide (KOH) in the proportion of 50% m/m. The reactions were stirred at room temperature and accompanied by thin layer chromatography (Scheme 1). After the reaction was complete, ice-cold distilled water was added and then neutralized with dilute hydrochloric acid (HCl). The resulting precipitate (**5**) was filtered and purified by slow recrystallization from acetone and isopropyl alcohol (3: 1), after drying. **Yield:** 62%. **Boiling point:** 231-234 °C. **¹H (DMSO-d₆, 500 MHz):** δ 8.26 (d, J = 8.90 Hz, H-2 e H-3, 2H), 8.11 (d, J = 8.90 Hz, H-4 e H-5, 2H), 8.02 (d, J = 2.54 Hz, H-18, 1H), 7.95 (ddd, J = 1.06 Hz, 1.70 Hz e 7.84 Hz, H-11), 7.76 (d, J = 15.87 Hz, H-8, 1H), 7.75-7.74 (m, H-12, 1H), 7.71 (dd, J = 2.54 Hz e 8.48 Hz, H-21, 1H), 7.67 (d, J = 8.48 Hz, H-19, 1H), 7.49 (dd, J = 7.84 Hz e 8.27 Hz, H-13, 1H), 7.41 (ddd, J = 1.06 Hz, 2.33 Hz e 8.27 Hz, H-14, 1H). **¹³C (DMSO-d₆, 500 MHz):** δ 188.92 (C-9), 148.57 (C-1), 141.98 (C-7), 138.62 (C-10), 136.77 (C-15), 135.00 (C-16), 134.70 (C-21), 132.15 (C-

Scheme 1: Synthesis of BSC



20), 130.50 (C-4 e C-5), 130.34 (C-18), 130.27 (C-17), 127.64 (C-19), 126.76 (C-6), 125.86 (C-11), 125.27 (C-8), 124.39 (C-2 e C-3), 124.24 (C-14), 118.85 (C-12). **IV:** 3218 (N-H), 1710 (C=O), 1342 (S=O), 1661 (Ar-CO-C=Ar), 1591-1472 (C-C_{Ar}), 1163 (Ar-Cl). **M (m/z):** 477.99376.

Crystallographic characterization. X-ray diffraction data of BSC were collected at room temperature using the Bruker APEX II CCD diffractometer with graphite-monochromated MoK α radiation ($\lambda=0.71073$ Å). The data were processed in the Bruker software SAINT²⁶ and the structure was solved and refined by direct and least square methods, respectively, throughout SHELX2014²⁷ software. All the hydrogen atoms were placed in calculated positions and refined with fixed individual displacement parameters [Uiso(H) = 1.2 Ueq or 1.5 Ueq] according to the riding model (C–H bond lengths of 0.97 Å and 0.96 Å for aromatic and methyl groups, respectively). The structural information (molecular representation, tables and figures) was obtained throughout the WinGX²⁸, Ortep²⁸ and Mercury²⁹ programs. The possible interactions and hydrogen bonds were checked by PARST³⁰ and PLATON³¹ software and analyzed from Hirshfeld surface.

Hirshfeld surface. Hirshfeld surface (HS) analysis was used to investigate the intermolecular interactions in the crystal packing of the BSC molecule and the associated 2D fingerprint plots were generated using the software Crystal Explorer 3.1.³² Spackman and coworkers^{33,34} have demonstrated how useful the Hirshfeld surfaces are and two-dimensional fingerprints derived from them characterize crystal packing, and allow understanding the spatial molecular relationships into crystal.³⁵ HS were developed to partition the space in molecular crystals for electron density integration purposes, this surface defines a region of space where the molecule electron density exceeds that of all neighboring molecules that is defined by $W(\mathbf{r}) = 0.5$, where W is a weight function, for a molecule in a crystal, derived from the atomic electron densities $\rho_i(\mathbf{r})$ ³⁶:

$$W(\mathbf{r}) = \frac{\sum_{i \in \text{molecule}} \rho_i(\mathbf{r})}{\sum_{i \in \text{crystal}} \rho_i(\mathbf{r})} \quad (1)$$

where the numerator is a sum of the atoms in the molecule of interest and the denominator is an analogous sum of the crystal³⁴. The analysis of the curvature can indicate the presence and nature of close contacts. Additionally, further information is gathered by mapping properties such as the electrostatic potential onto these surfaces³⁵. Consequently, for this analysis, the normalized contact distances (d_{norm}) are defined in terms of the distances from the HS to the nearest nucleus inside the surface (d_i) and outside the surface, (d_e) and the van der Waals radii of the atoms. d_{norm} is given by

$$d_{\text{norm}} = \frac{(d_i - r_i^{\text{vdW}})}{r_i^{\text{vdW}}} + \frac{(d_e - r_e^{\text{vdW}})}{r_e^{\text{vdW}}} \quad (2)$$

where r_i^{vdW} and r_e^{vdW} are the van der Waals radii³⁷. HS uses colors to represent the interactions with distances that are closer, equal or longer to the sum of the van der Waals radii

graphically representing them by red, white and blue areas, respectively.

Optimization and assignments. The starting geometry used in the calculations was taken directly from the X-ray data and was fully optimized without constraint using density functional theory (DFT) as implemented in the Gaussian 09 package of programs³⁸. The functional M06-2X³⁹ was employed throughout the calculations, alongside the extended Gaussian basis set 6-311+G(d,p). The harmonic frequencies were calculated at the same level of theory to confirm that the optimized geometry was found in a local minimum. These calculations showed that there are no imaginary frequencies for the optimized structure; the absence of imaginary frequencies confirms that the optimized structure is truly in a local minimum. The assignments of the vibrational frequencies were carried out by potential energy distribution (PED) analysis using VEDA 4 software and were supported by the animation option of Gaussview⁴⁰.

Structure-based pharmacophoric screening. PharmMapper is a web server for prediction of potential biological activities against any given small molecule using a structure-based pharmacophore mapping approach. This automatically predicts the best mapping poses for a given query molecule against all the pharmacophore models in PharmTargetDB and lists the best-fitted biological targets with their respective scores^{41,42}. Briefly, the 3D structure of BSC in Mol2 format was submitted to PharmMapper. During the procedure, the maximum conformations were set up to 300, and the number of reserved matched targets was 300. Other parameters were kept as default.

ChEMBL analysis. Substructure searching of the chalcone scaffold (1,3-diphenyl-2-propen-1-one) was performed in the ChEMBL database using the Sketch tool. This chemical searching yielded 1,416 compounds that are active (IC_{50} , K_i , or $K_d \leq 10 \mu M$) against at least one of 263 found biological targets. Further, we note that 22 of these biological targets also were available on PharmMapper list (see Supplementary Table S2), increasing the reliability of our predictions. Therefore, only targets found in both approaches (ChEMBL and PharmMapper) were carried on for further analyses.

Molecular docking. The structure of BSC was imported into the Maestro workspace v.9.3 and prepared using LigPrep 2.5 (Schrödinger, LCC, New York, 2012). Subsequently, 1000 conformations were generated using OMEGA v.2.5.1⁴³, while AM1-BCC charges⁴⁴ were added using QUACPAC v.1.6.3. In parallel, 3D structures of selected targets were imported from the Protein Data Bank (PDB) database⁴⁵ and pre-processed using Protein Preparation Wizard available on the Maestro workspace (Schrödinger LLC). During protein preparation, hydrogen atoms were first added to the proteins, and bond orders and formal charges were adjusted. Missing side chains and loops were predicted using Prime v.3.1 (Schrödinger LLC). The protonation states of polar amino acids were predicted by PROPKA v.3.1 (Schrödinger LLC)⁴⁶ at neutral and acid (only for

proteases) pHs. Subsequently, full-atom protein structure minimization using the OPLS-2005 force field was carried out⁴⁷. The prepared proteins were then subjected to the grid-generation protocol using two different binding site detection strategies. In the first strategy, grids were generated using a molecular probe for detection of pockets around the proteins that could potentially be allosteric binding sites. In the second strategy, co-crystallized ligands were considered geometric centers of the grids. Grid information is available in Table S1. After grid generation, molecular docking studies were performed using the high-resolution protocol from FRED and HYBRID programs, both available on OEDocking suite v.3.2.0^{48,49}, and the ChemGauss4 score function. Finally, a consensus score was created by averaging the predicted values from the individual docking programs, providing better predictive ability as compared to the individual scores.

Evaluation of cytotoxicity. Cytotoxicity analysis of the 2,5-dichloro-N-{3-[(2E)-3-(4-nitrophenyl)prop-2-enoyl]phenyl}benzenesulfonamide (BSC) was performed using the MTT method, colorimetric analysis, based on the conversion of the tetrazolium 3-(4,5-dimethyl-2-thiazole)-2,5-diphenyl-2-H-bromide salt (MTT) in formazan blue, from mitochondrial enzymes present only in metabolically active cells.

The tumor cells used, SF-295 (human glioblastoma), PC-3 (prostate cancer) and HCT-116 (colon cancer) were donated by the National Cancer Institute (USA) and cultured in RPMI 1640 medium supplemented with 10% of fetal bovine serum antibiotics Streptomycin and penicillin at 1%, incubated at 37°C and an atmosphere containing 5% of CO₂. The tested compound was diluted into sterile and pure DMSO at 5 mg.mL⁻¹. For IC₅₀ determination, the samples were tested at increasing concentrations (0,39 to 52,37 μM) in serial dilutions.

Cells were plated at 0.1 x 10⁶ cells/ml for SF-295 and PC-3 and 0.7 x 10⁵ cells/ml for HCT-116 lineage. The plates were incubated for 72 hours at 5% CO₂ and 37°C. At the end of this, they were centrifuged and the supernatant removed. Then, 150 μL of the MTT solution (tetrazolium salt) was added and the plates were incubated for 3h. The absorbance was read after dissolution of the precipitate with 150 μL of pure DMSO in a plate spectrophotometer at 595 nm. Doxorubicin was used as positive control at concentrations from 0,06 to 8,62 μM.

Results

Solid state characterization

The analyzed structure is a hybrid compound 2,5-dichloro-N-{3-[(2E)-3-(4-nitrophenyl)prop-2-enoyl]phenyl}benzenesulfonamide (BSC) derived from sulfonamide chalcone. Its molecular structure is composed by a nitrophenyl group connected at the chalcone moiety and a sulfonamide group at the *meta* position of the aromatic chalcone ring. The sulfonamide group possesses two chloro atoms at *meta* and *orto* positions. Additionally, this molecule has an E conformation in relation the double bond C7–C8 in conjugation to carbonyl group. This sulfonamide chalcone crystallized in the monoclinic space group C2/c with a single

ARTICLE

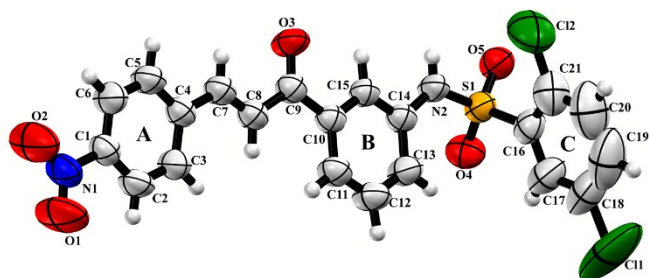


Figure 1: Ortep representation with ellipsoids at 60% of probability and numbering scheme of BSC. Hydrogen atoms are represented by spheres with arbitrary radii.

independent molecule in the asymmetric unit and consequently eight molecules in unit cell. Although the residual electronic density indicated the presence of solvent, its refinement was not successful and we chose to treat it as void. The unit cell metrics are: $a = 22.2982(18) \text{ \AA}$, $b = 8.5917(8) \text{ \AA}$ and $c = 26.0739(14) \text{ \AA}$, $\alpha = \gamma = 90^\circ$ and $\beta = 112.116(5)^\circ$. The main crystallographic parameters are shown at Table 1, followed by Ortep representation of BSC in Figure 1. The nitro group has a positional disorder, in which the second conformation has a 39.71% occupancy factor and was handled separately of the first one conformation. In this way, the whole discussion is based on the dominant conformation.

In the first place, the quasi planarity of the chalcone portion is confirmed by the angle of 5.23° formed between the planes of its aromatic rings, whereas the sulfonamide moiety is almost perpendicular to it (85.72°). Besides the interplanar angles, the chalcone moiety flatness is confirmed by the dihedral angles $\tau_2 - \tau_4$, corresponding to rotations around single bonds C4-C7, C8-C9 and C9-C10, respectively (Table 2). On other hand, planarity deviations are noted near to nitro (τ_1), sulfone (τ_6) and dichlorobenzene groups (τ_7). The olefin portion has a synperiplanar conformation regarding the amino group, while the Cl2 atom has a synclinal conformation regarding to the plane formed by atoms N2, S1 and C16. A search made in the Mogul software revealed that the dihedral angle τ_6 is unusual, since out of 898 hits analysed, only 16 (1.78%) had similar values.

Table 1: Crystal data and structure refinement for BSC

Empirical Formula	$C_{21}H_{14}Cl_2SN_2O_5$
Formula Weight	477.30 g/mol
Temperature	296 K
Wavelength	0.7103 \AA
Crystal system, space group, Z	Monoclinic, C2/c
Unit cell dimension	$a = 22.2982(18) \text{ \AA}$, $\alpha = 90^\circ$ $b = 8.5917(8) \text{ \AA}$, $\beta = 112.116(5)^\circ$ $c = 26.0739(14) \text{ \AA}$, $\gamma = 90^\circ$
Volume	$4627.7(6) \text{ \AA}^3$
Z, calculated density	8, 1.370 mg/m ³
Absorption coefficient	0.405 mm ⁻¹
F (000)	1952
Reflections collected / unique	26695 / 4793 [R(int) = 0.0330]
Refinement method	Full-matrix least-squares on F ²
Goodness-of-fit on F ²	1.067
Final R indices [I > 2σ(I)]	$R_1 = 0.0579$, $wR_2 = 0.1490$
R indices (all data)	$R_1 = 0.0923$, $wR_2 = 0.1699$

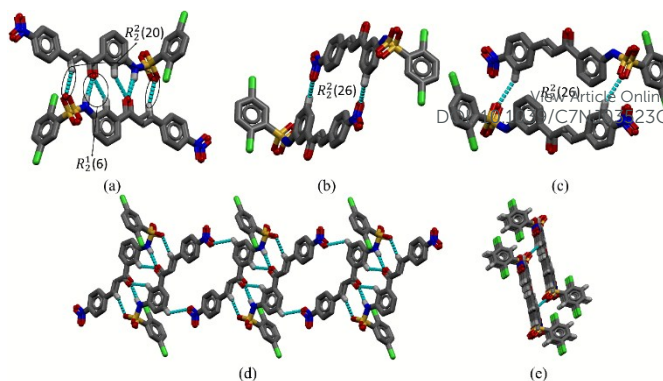


Figure 2: Intermolecular interactions of BSC. Dimers formed by interactions C15-H15...O3...N2-HN1 and C7-H7...O5 (a), C12-H12...O1 (b) and C2-H2...O4 (c) are shown. In addition, the 1D chain formed is shown in (d), while the stacking of layers is shown in (e).

In total, there are three non-classical H-bonds (C7-H7...O5, C2-H2...O4, C12-H12...O1) and one bifurcated (C15-H15...O3...N2-HN1) in which two donors compete for the same receptor, as can be seen in Figure 2 (quantitative data are tabulated in Table 3).

The crystal packing of BSC is stabilized by dimers, as seen in Figures 2 a-c. The interactions C15-H15...O3...N2-HN1 join two BSC molecules in a $R_2^2(6)$ ring motif, while C7-H7...O5 gives rise to a $R_2^2(20)$ ring motif involving carbonyl and amine groups, both forming a H-bonded dimer (dimer 1, Figure 2a). A series of $R_2^2(26)$ ring motifs are present in the dimers involving nitro (dimer 2, Figure 2b) and sulfone (dimer 3, Figure 2c) groups. Hydrogen bonded dimers are linked in a chain by a C-H...O interaction, involving the nitrobenzene aromatic ring (Figure 2d). These chains form a layer associated by interactions around sulfone and nitro groups. The crystal packing is obtained by stacking these dimeric chains, intercalating chalcone moieties and sulfonamides aromatic rings. Solvent accessible voids with 13.2% of unit cell volume were observed, which is compatible with an acetone solvent, as seen in Figure S1.

The intermolecular interactions of BSC (donor and acceptor regions) were quantitatively analyzed by normalized Hirshfeld surface d_{norm} . Since Hirshfeld surfaces are calculated from electronic density, this was made before squeeze routine. This surface shows the intermolecular interactions, where hot colors indicate the presence of higher intensities and cold colors indicate the presence of lower intensity. The signals from the first dimer interactions (Figure 3a), showed different intensities for N2-HN1...O3 (I), C15-H15...O3 (II) and N7-H7...O5 (III) interactions. The higher intensity on the interaction involving the amino group indicates a greater force in this region, matching the higher energy of hydrogen bonds. When then compared to the other dimers stabilized by the C12-H12...O1 (IV) and C2-H2...O4 (V) interactions, and inferred that dimer 1 has greater effectiveness in the crystalline packing of BSC.

Table 2: Main torsion angles of BSC

Involved atoms	Angle	Value (°)
O1-N1-C1-C2	τ_1	5.4(3)
C3-C4-C7-C8	τ_2	1.6(6)
C7-C8-C9-C10	τ_3	174.2(3)
C8-C9-C10-C15	τ_4	177.1(3)
C15-C14-N2-S1	τ_5	178.2(2)
C14-N2-S1-C16	τ_6	-69.7(3)

Table 3: Hydrogen bonds involved in crystal packing of BSC

N	D-H...A	dD-H(Å)	dH...A(Å)	dD...A (Å)	\angle D-H...A (°)	Symmetry code
1	C7-H7...O5	0.897	2.568	3.430	161.49	-x,1-y,-z
2	C2-H2...O4	0.878	2.694	3.488	151.05	1/2-x,1/2-y,-z
3	C12-H12...O1	0.963	2.707	3.272	118.08	1/2-x,-1/2-y,-z
4	C15-H15...O3	0.955	2.506	3.288	139.04	-x,1-y,-z
5	N2-HN1...O3	0.826	2.105	2.890	158.64	-x,1-y,-z

Assignments

Table 4 shows the main IR intensities, the experimental and calculated vibrational frequencies for the optimized geometry and the proposed vibrational assignments for BSC, while the spectrum (experimental and theoretical, overlapped) is presented in Figure 4.

For the sake of clarity, will be discussed only the values for the main absorbing groups. To correct the systematic overestimation of the vibrational frequencies of the DFT methods was applied a scaling factor of 0.940⁵⁰.

The DFT results for $\nu(\text{CH})_{\text{aromatic}}$ are in the range of 3029 to 3074 cm^{-1} and experimental values were in the range of 3046–3071 cm^{-1} . Concerning to the experimental values of $\nu(\text{C}-\text{C})_{\text{aromatic}}$ stretches absorptions were found in 1612 cm^{-1} and 1473 cm^{-1} , while DFT results are 1597.75 cm^{-1} and 1326.98 cm^{-1} .

The carbonyl stretching vibrations occur at 1581 cm^{-1} in DFT and 1661 cm^{-1} in IR spectra, while the calculated wavenumber

for the C=O vibration results at 1644 cm^{-1} , while in experimental IR the value is 1713 cm^{-1} .

The calculated N–H stretching vibration for BSC is one band at about 3367 cm^{-1} and for $\beta\text{N-H}$ is 1410 cm^{-1} . In the IR spectra, these values are 3220 cm^{-1} and 1521 cm^{-1} , respectively. Still, the C–N stretching modes vibrations is observed at 1344 cm^{-1} in the IR experimental spectrum and at 1218 cm^{-1} in theoretical. Whereas the theoretical wavenumbers of C–Cl stretching vibration is 582 cm^{-1} and the calculated value is 544 cm^{-1} .

The assignment of thiocarbonyl group in our DFT calculations appears in 977 cm^{-1} , while in the IR spectra this value is 962 cm^{-1} . In its turn, the SO₂ asymmetric and symmetric stretches are calculated at 1252 cm^{-1} and 1078 cm^{-1} , respectively. In experimental IR, these bands appear at 1249 cm^{-1} and 1163 cm^{-1} , respectively. Likewise, the vibrational spectral modes of S–N vibration was calculated at 797 cm^{-1} and the experimental value was obtained at 900 cm^{-1} .

The NO₂ stretching vibrations give two strong bands (asymmetric and symmetric), in BSC, 1519 cm^{-1} and 1342 cm^{-1} are, respectively, the values in the IR spectrum, while 1500 cm^{-1} and 1325 cm^{-1} are, respectively, the theoretical values. To conclude, the bands at 847 cm^{-1} and 846 cm^{-1} in this paper are assigned to the ρNO_2 mode in theoretical calculations and experimental IR, respectively.

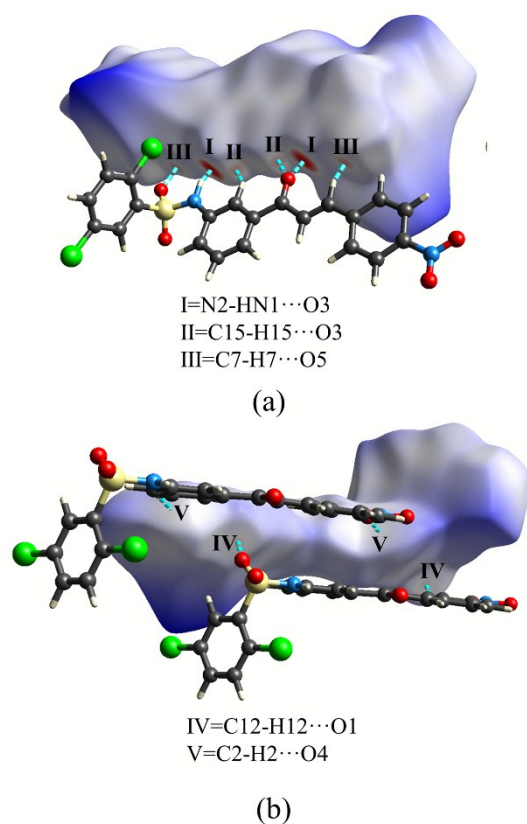


Figure 3: d_{norm} Hirshfeld surface of BSC showing intermolecular interactions involved in crystal packing.

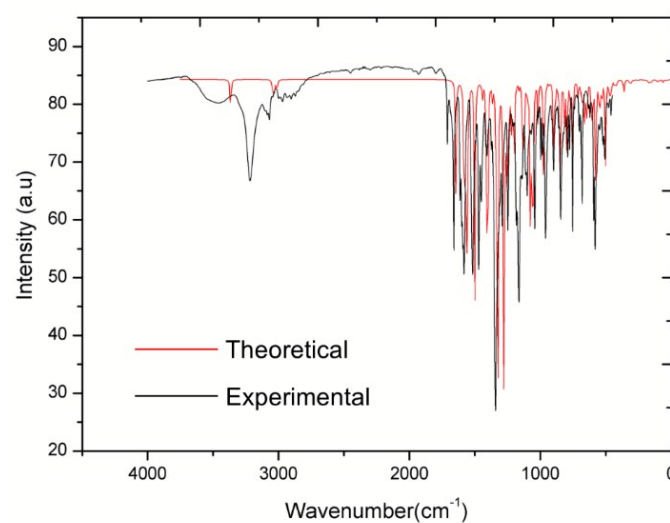


Figure 4: Experimental (KBr) (black) and theoretical (red) IR spectra of BSC

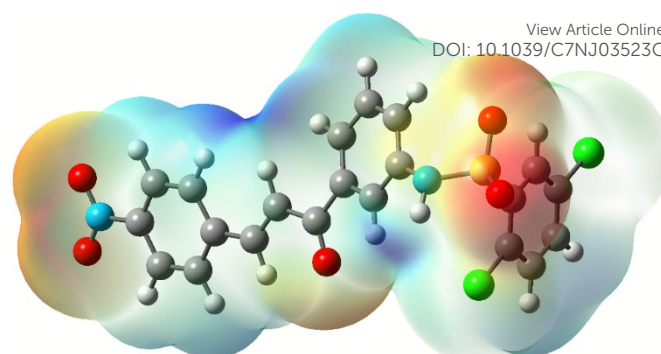
Table 4: Vibrational assignments and wave numbers (cm^{-1}) calculated, with M06-2X/6-311+G(d,p), to $\text{C}_{21}\text{H}_{14}\text{Cl}_2\text{N}_2\text{O}_5\text{S}$

	Unscaled IR freq.	Scaled IR freq. ^a	Intensity ^b	IR observed ^c
$\nu(\text{CH})_{\text{aromatic}}$	3222.97 to 3242.00	3029.59 to 3074.48	4.70 to 13.90	3046 to 3071
$\nu(\text{C}-\text{C})_{\text{aromatic}}$	1669.74 to 1411.68	1597.75 to 1326.98	22.77 to 169.97	1612 to 1473
$\nu \text{C}=\text{C}$	1682.41	1581.46	191.61	1661
$\nu \text{C}=\text{O}$	1749.93	1644.93	116.83	1713
$\nu \text{N}-\text{H}$	3582.29	3367.35	44.28	3220
$\beta \text{N}-\text{H}$	1500.30	1410.28	186.36	1521
$\nu \text{C}-\text{NH}$	1296.53	1218.74	81.82	1344
$\nu \text{C}-\text{Cl}$	579.57	544.79	21.16	582
$\nu \text{C}-\text{S}$	1039.68	977.30	96.01	962
$\nu_{\text{asym}} \text{SO}_2$	1332.55	1252.60	103.68	1249
$\nu_{\text{sym}} \text{SO}_2$	1146.88	1078.07	134.42	1163
$\nu \text{S}-\text{N}$	847.94	797.06	78.45	900
$\nu_{\text{asym}} \text{NO}_2$	1596.31	1500.53	233.64	1519
$\nu_{\text{sym}} \text{NO}_2$	1410.49	1325.40	289.52	1342
ρNO_2	901.42	847.33	124.47	846

Molecular electrostatic potential map and frontier molecular orbitals

The molecular electrostatic potential (MEP) map on a surface can be a positive or negative quantity. It is positive if the positive charges (nuclei) dominate over the negative charge (electrons). The MEP is generally visualized through the mapping of its values onto the molecular surface reflecting the molecular boundary. The MEP is a very powerful tool to describe molecular sites of electrophilic attack, nucleophilic reactions and hydrogen bonding interaction. In addition, MEP is very used to describe drug-receptor and enzyme-substrate interactions, because it is a force that acts on long distance⁵¹. As MEP is an observable reflection of the wavefunction, it can be determined experimentally by diffraction or by computational methods. Figure 5 shows the MEP surface calculated, showing regions that are well distinguished, using M06-2X/6-311+G(d,p) level of theory for the BSC in gas-phase. The negative MEP (red color in Figure 5) corresponds to the areas of high electron density; which are in the site of O atoms in SO_2 , $\text{C}=\text{O}$ and NO_2 groups. The positive MEP (blue color in Figure 5) corresponds to the areas of high depleted electron density; which are the site of H3 bounded C3 and HN1 bounded N1.

In addition, Figure 6 displays a graphical representation of the HOMO (Highest Occupied Molecular Orbital) and LUMO (Lowest Unoccupied Molecular Orbital) frontier molecular orbitals calculated under a M06-2X/6-311+G(d,p) level of theory. The HOMO ($E = -8.58 \text{ eV}$) orbital that presents π^* -bonding symmetry, is located mainly at the aromatic ring substituted with a benzenesulfonamide group. Figure 6(b) shows that the LUMO ($E = -2.66 \text{ eV}$) molecular orbital presents π -antibonding symmetry, located along to $\text{C}=\text{O}$, $\text{C}=\text{C}$ and nitrobenzene ring. The gap energy (E_{Gap}), hardness (η) and softness (σ) values were calculated using the equations⁵²

**Figure 5:** Molecular electrostatic potential map of BSC

$$E_{\text{Gap}} = E_{\text{LUMO}} - E_{\text{HOMO}} \quad (3)$$

$$\eta = \frac{-(E_{\text{HOMO}} - E_{\text{LUMO}})}{2} \quad (4)$$

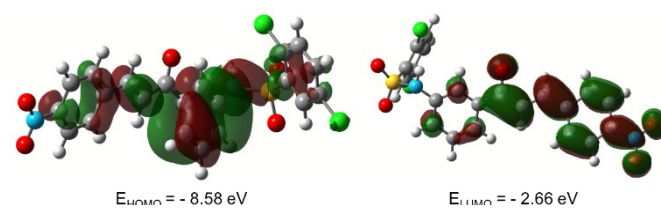
$$\sigma = \frac{-2}{(E_{\text{HOMO}} - E_{\text{LUMO}})} \quad (5)$$

with values of 5.92 eV, 2.96 eV and 0.34 eV, respectively. These high values indicate a high chemical stability and high first excitation energies for the compound.

Potential biological activities for BSC

Potential biological activities of BSC were predicted using two different approaches as described in the methods. Initially, the top 300 potential protein targets of BSC were predicted using PharmMapper server. In parallel, 263 potential targets also were identified by substructure search in ChEMBL database. Finally, to improve the specificity, a total of 22 potentially interacting targets identified in both sets of results were selected for further investigation (Table S2).

To further characterize the binding modes and interaction scores of BSC with predicted protein targets, molecular docking studies were performed using FRED and HYBRID programs. FRED performs an exhaustive search, by systematically searching rotations and translations of each conformer of the ligand within the active site, filtering the possible poses for shape complementarity and pharmacophoric features before selecting and optimizing poses using the Chemgauss4 scoring function. Like FRED, HYBRID performs a systematic, exhaustive, non-stochastic examination of poses within the protein binding site. However, HYBRID reduces this search space based on shape and chemical complementarity to known bound ligands.

**Figure 6:** Frontier molecular orbitals of BSC followed by calculated HOMO, LUMO and band-gap.

The scores of docking analysis are shown in Tables S2 and 5. From the consensus docking scores, we suggest that the BSC can act as an anticancer agent by interacting with nuclear retinoic acid receptors alpha (RAR α , score = -16.08) and beta (RAR β , score = -17.45). Due to these excellent docking scores, we suggest that BSC may be investigated as a potential anticancer agent. The proposed biological activity is based on following observations: (i) chalcone derivatives are known RARs agonists with IC_{50s} in the nanomolar range^{53–55}; (ii) the RARs interact with many different coactivator and corepressor proteins to regulate transcription⁵⁶; and (iii) the binding of retinoids to RARs induce apoptosis in various human cancer cells⁵⁶.

Figure 7 illustrates the binding of BSC into the active sites of RARs identified as their potential targets. Like in all retinoid complexes (see co-crystallized ligands in Supplementary Figure S1), the nitro moiety of the ligand is anchored by a network of hydrogen bonds with a water molecule, and the sidechains of Arg276 and Ser287. In addition, this structural analysis shows that the predicted binding modes allow several hydrophobic interactions between the phenyl rings of the ligand with residues Phe228, Ile236, Leu398, Leu 414, Leu306, Cys265, Ile271, Leu269, Phe302, and Ile273.

Experimental validation

To evaluate the predicted anticancer activity of BSC, we investigated its inhibitory effects on a three cancer cells. Doxorubicin was used as positive control. Inhibitory percentage was 92.47 (\pm 0.32), 99.97 (\pm 2.21) and 97.73 (\pm 1.37 for PC-3, HCT-116, and SF-295, respectively). Results showed that BSC exhibited remarkable inhibitory effect on cell growth with IC_{50s} of 10.84 (8.39–14.01) μ M, 5.39 (4.24–6.86) μ M, and 13.16 (11.78–14.69) μ M in PC-3, HCT-116, and SF-295, respectively.

Conclusions

The main results showed that the BSC compound has a planar conformation in its chalcone portion, corroborated by the low angle formed between the aromatic rings (5.23°). This planarity

Table 5: Top five predicted targets

Predicted biological target (organism)	PharmMapper fit score	FRED score	HYBRID score	Consensus score
Retinoic acid receptor β (Homo sapiens)	3.86	-17.78	-17.12	-17.45
Retinoic acid receptor α (Homo sapiens)	3.68	-16.46	-15.70	-16.08
Aldose reductase (Homo sapiens)	2.85	-13.67	-10.33	-12.00
Dihydrofolate reductase (Homo sapiens)	3.46	-13.20	-9.93	-11.56
Phosphodiesterase 4D (Homo sapiens)	4.89	-11.64	-11.30	-11.47

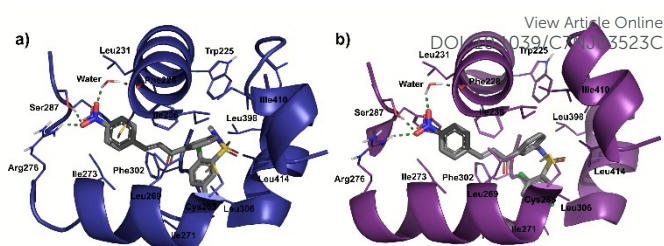


Figure 7: Intermolecular interactions of RAR α (a) and RAR β (b) with BSC

is expected for the chalcone backbone, since the aromatic rings and the carbonyl, nitro, and olefin groups form a conjugate system. In addition, intermolecular interactions of type C-H...O and N-H...O form a dimeric supramolecular arrangement, as confirmed from Hirshfeld surface analysis and molecular potential maps for BSC. Regarding molecular stability of BSC, the calculated gap energy ($E_{\text{Gap}}=5.92$ eV), hardness ($\eta=2.96$ eV) and softness ($\sigma=0.34$ eV) indicates a high chemical stability and high first excitation energies for analyzed compound. The results of inverse virtual screening approach and experimental testing allowed identifying potential biological applications for BSC. Based on this approach, we found that BSC might interact with binding sites of the RAR α and RAR β .

Conflicts of interest

There are no conflicts to declare.

Acknowledgements

The authors would like to thank Brazilian funding agencies CNPq, CAPES, and FAPEG for financial support and fellowships. Also, the authors are grateful to OpenEye Scientific Software Inc. (<https://www.eyesopen.com/>) for providing academic license of their softwares and to Raquel Ferreira Naves for RMN analysis. Single crystal X-ray diffraction data were collected at Physics Institute of the Federal University of Goiás. Pedro Cravo and Hamilton B. Napolitano are research fellows of the Conselho Nacional de Desenvolvimento Científico e Tecnológico (CNPq) of Brazil.

Notes and references

- 1 D. J. Newman and G. M. Cragg, *J. Nat. Prod.*, 2016, **79**, 629–661.
- 2 J. Eder, R. Sedrani and C. Wiesmann, *Nat. Rev. Drug Discov.*, 2014, **13**, 577–587.
- 3 K. C. Morrison and P. J. Hergenrother, *Nat. Prod. Rep.*, 2014, **31**, 6–14.
- 4 C. Zhuang, W. Zhang, C. Sheng, W. Zhang, C. Xing and Z. Miao, *Chem. Rev.*, 2017, **117**, 7762–7810.
- 5 D. ISRAF, T. KHAIZURIN, A. SYAHIDA, N. LAJIS and S. KHOZIRAH, *Mol. Immunol.*, 2007, **44**, 673–679.
- 6 N. Aoki, M. Muko, E. Ohta and S. Ohta, *J. Nat. Prod.*, 2008, **71**, 1308–1310.
- 7 R. B. Birari, S. Gupta, C. G. Mohan and K. K. Bhutani,

- 8 *Phytomedicine*, 2011, **18**, 795–801.
- 9 M. Chen, S. B. Christensen, J. Blom, E. Lemmich, L. Nadelmann, K. Fich, T. G. Theander and A. Kharazmi, *Antimicrob. Agents Chemother.*, 1993, **37**, 2550–2556.
- 10 S. Cho, S. Kim, Z. Jin, H. Yang, D. Han, N.-I. Baek, J. Jo, C.-W. Cho, J.-H. Park, M. Shimizu and Y.-H. Jin, *Biochem. Biophys. Res. Commun.*, 2011, **413**, 637–642.
- 11 T. Yamamoto, M. Yoshimura, F. Yamaguchi, T. Kouchi, R. Tsuji, M. Saito, A. Obata and M. Kikuchi, *Biosci. Biotechnol. Biochem.*, 2004, **68**, 1706–11.
- 12 Y. Sato, J.-X. He, H. Nagai, T. Tani and T. Akao, *Biol. Pharm. Bull.*, 2007, **30**, 145–149.
- 13 V. R. Solomon and H. Lee, *Biomed. Pharmacother.*, 2012, **66**, 213–220.
- 14 D. W. Kim, M. J. Curtis-Long, H. J. Yuk, Y. Wang, Y. H. Song, S. H. Jeong and K. H. Park, *Food Chem.*, 2014, **153**, 20–27.
- 15 I. M. PRLINA, C. P. DAHLEN and A. J. BISCHOFF, *Antibiot. Med. Clin. Ther. (New York, NY)*, 1958, **5**, 242–250.
- 16 B. P. Ryan, *Med. J. Aust.*, 1975, **1**, 101–103.
- 17 A. DOUGLAS, R. HALL, D. B. HORN, D. N. KERR, D. T. PEARSON and H. RICHARDSON, *Br. Med. J.*, 1961, **2**, 206–210.
- 18 S. K. Bhattia, D. R. Hadden, D. A. Montgomery and J. A. Weaver, *Br. Med. J.*, 1970, **2**, 570–572.
- 19 S. SOLOMON and A. HIRANO, *Neurology*, 1959, **9**, 167–170.
- 20 E. J. Hammond, R. J. Perchalski, B. J. Wilder and J. R. McLean, *Gen. Pharmacol.*, 1987, **18**, 303–307.
- 21 A. Markham, *Drugs*, 2017, **77**, 697–704.
- 22 T. D. Penning, J. J. Talley, S. R. Bertenshaw, J. S. Carter, P. W. Collins, S. Docter, M. J. Graneto, L. F. Lee, J. W. Malecha, J. M. Miyashiro, R. S. Rogers, D. J. Rogier, S. S. Yu, G. D. Anderson, E. G. Burton, J. N. Cogburn, S. A. Gregory, C. M. Koboldt, W. E. Perkins, K. Seibert, A. W. Veenhuizen, Y. Y. Zhang and P. C. Isakson, *J. Med. Chem.*, 1997, **40**, 1347–1365.
- 23 J. C. Adkins and D. Faulds, *Drugs*, 1998, **55**, 837–844.
- 24 S. Iftikhar, S. Khan, A. Bilal, S. Manzoor, M. Abdullah, A.-H. Emwas, S. Sioud, X. Gao, G. A. Chotana, A. Faisal and R. S. Z. Saleem, *Bioorg. Med. Chem. Lett.*, 2017, **27**, 4101–4106.
- 25 B. R. A. Tawna L. Whited, Christopher R.T. Stang, R. S. Khupse, R. W. Dudley and R. A. Schneider, *FASEB J.*, 2016, **30**, 515.
- 26 L. D. Pennington, M. D. Croghan, K. K. C. Sham, A. J. Pickrell, P. E. Harrington, M. J. Frohn, B. A. Lanman, A. B. Reed, M. R. Lee, H. Xu, M. McElvain, Y. Xu, X. Zhang, M. Fiorino, M. Horner, H. G. Morrison, H. A. Arnett, C. Fotsch, A. S. Tasker, M. Wong and V. J. Cee, *Bioorg. Med. Chem. Lett.*, 2012, **22**, 527–531.
- 27 Bruker (2012). APEX. Bruker AXS Inc., Madison, Wisconsin, USA.
- 28 G. M. Sheldrick, *Acta Crystallogr. Sect. C*, 2015, **71**, 3–8.
- 29 L. J. Farrugia, *J. Appl. Crystallogr.*, 2012, **45**, 849–854.
- 30 C. F. Macrae, I. J. Bruno, J. a. Chisholm, P. R. Edgington, P. McCabe, E. Pidcock, L. Rodriguez-Monge, R. Taylor, J. van de Streek and P. a. Wood, *J. Appl. Crystallogr.*, 2008, **41**, 466–470.
- 31 M. Nardelli, *J. Appl. Crystallogr.*, 1995, **28**, 659–659.
- 32 A. L. Spek, *J. Appl. Crystallogr.*, 2003, **36**, 7–13.
- 33 J. J. McKinnon, M. J. Turner, D. Jayatilaka, M. A. Spackman, D. J. Grimwood and S. K. Wolff, 2012.
- 34 M. A. Spackman and J. J. McKinnon, *CrystEngComm*, 2002, **4**, 378–392.
- 35 M. A. Spackman and D. Jayatilaka, 2009, 19–32.
- 36 G. J. O. Beran, *Chem. Rev.*, 2016, **116**, 5567–5613.
- 37 C. Jelsch, K. Ejsmont and L. Huder, *IUCrJ*, 2014, **1**, 119–128.
- 38 B. Chattopadhyay, A. K. Mukherjee, N. Narendra, H. P. Hemantha, V. V. Sureshababu, M. Helliwell and M. Mukherjee, *Cryst. Growth Des.*, 2010, **10**, 4476–4484.
- 39 M. J. Frisch, G. W. Trucks, H. B. Schlegel, G. E. Scuseria, M. A. Robb, J. R. Cheeseman, G. Scalmani, V. Barone, B. Mennucci, G. A. Petersson, H. Nakatsuji, M. Caricato, X. Li, H. P. Hratchian, A. F. Izmaylov, J. Bloino, G. Zheng, J. L. Sonnenberg, M. Hada, M. Ehara, K. Toyota, R. Fukuda, J. Hasegawa, M. Ishida, T. Nakajima, Y. Honda, O. Kitao, H. Nakai, T. Vreven, J. A. Montgomery Jr., J. E. Peralta, F. Ogliaro, M. Bearpark, J. J. Heyd, E. Brothers, K. N. Kudin, V. N. Staroverov, R. Kobayashi, J. Normand, K. Raghavachari, A. Rendell, J. C. Burant, S. S. Iyengar, J. Tomasi, M. Cossi, N. Rega, J. M. Millam, M. Klene, J. E. Knox, J. B. Cross, V. Bakken, C. Adamo, J. Jaramillo, R. Gomperts, R. E. Stratmann, O. Yazyev, A. J. Austin, R. Cammi, C. Pomelli, J. W. Ochterski, R. L. Martin, K. Morokuma, V. G. Zakrzewski, G. A. Voth, P. Salvador, J. J. Dannenberg, S. Dapprich, A. D. Daniels, Ö. Farkas, J. B. Foresman, J. V. Ortiz, J. Cioslowski and D. J. Fox, *Gaussian Inc Wallingford CT*, 2009, 34, Wallingford CT.
- 40 Y. Zhao and D. G. Truhlar, *Theor. Chem. Acc.*, 2008, **120**, 215–241.
- 41 R. Dennington, T. Keith, J. Millam, R. , Dennington, T. Keith and J. Millam, 2009.
- 42 X. Liu, S. Ouyang, B. Yu, Y. Liu, K. Huang, J. Gong, S. Zheng, Z. Li, H. Li and H. Jiang, *Nucleic Acids Res.*, 2010, **38**, W609–W614.
- 43 X. Wang, C. Pan, J. Gong, X. Liu and H. Li, *J. Chem. Inf. Model.*, 2016, **56**, 1175–1183.
- 44 P. C. D. Hawkins, A. G. Skillman, G. L. Warren, B. A. Ellingson and M. T. Stahl, *J. Chem. Inf. Model.*, 2010, **50**, 572–584.
- 45 A. Jakalian, D. B. Jack and C. I. Bayly, *J. Comput. Chem.*, 2002, **23**, 1623–1641.
- 46 P. W. Rose, A. Plić, C. Bi, W. F. Bluhm, C. H. Christie, S. Dutta, R. K. Green, D. S. Goodsell, J. D. Westbrook, J. Woo, J. Young, C. Zardecki, H. M. Berman, P. E. Bourne and S. K. Burley, *Nucleic Acids Res.*, 2015, **43**, D345–56.
- 47 C. R. Søndergaard, M. H. M. Olsson, M. Rostkowski and J. H. Jensen, *J. Chem. Theory Comput.*, 2011, **7**, 2284–2295.
- 48 J. L. Banks, H. S. Beard, Y. Cao, A. E. Cho, W. Damm, R. Farid, A. K. Felts, T. A. Halgren, D. T. Mainz, J. R. Maple, R. Murphy, D. M. Philipp, M. P. Repasky, L. Y. Zhang, B. J. Berne, R. A. Friesner, E. Gallicchio and R. M. Levy, *J. Comput. Chem.*, 2005, **26**, 1752–1780.
- 49 M. McGann, *J. Comput. Aided. Mol. Des.*, 2012, **26**, 897–906.
- 50 M. McGann, *J. Chem. Inf. Model.*, 2011, **51**, 578–596.

Journal Name

ARTICLE

- 50 R. Paciotti, C. Coletti, N. Re, D. Scuderi, B. Chiavarino, S. Fornarini and M. E. Crestoni, *Phys. Chem. Chem. Phys.*, 2015, **17**, 25891–25904.
- 51 R. R. Ternavisk, A. J. Camargo, F. B. C. Machado, J. A. F. F. Rocco, G. L. B. Aquino, V. H. C. Silva and H. B. Napolitano, *J. Mol. Model.*, 2014, **20**, 2526.
- 52 S. S. Oliveira, L. G. Santin, L. R. Almeida, L. A. Malaspina, C. Lariucci, J. F. Silva, W. B. Fernandes, G. L. B. Aquino, R. Gargano, A. J. Camargo and H. B. Napolitano, *J. Mol. Model.*, 2017, **23**, 35.
- 53 S. Álvarez, R. Álvarez, H. Khanwalkar, P. Germain, G. Lemaire, F. Rodríguez-Barrios, H. Gronemeyer and Ángel R. de Lera, *Bioorg. Med. Chem.*, 2009, **17**, 4345–4359.
- 54 B. P. Klaholz, A. Mitschler and D. Moras, *J. Mol. Biol.*, 2000, **302**, 155–170.
- 55 H. Kagechika, E. Kawachi, Y. Hashimoto and K. Shudo, *J. Med. Chem.*, 1989, **32**, 834–840.
- 56 X. Tang and L. J. Gudas, *Annu. Rev. Pathol. Mech. Dis.*, 2011, **6**, 345–364.

View Article Online
DOI: 10.1039/C7NJ03523C